Cell Differentiation and Aging Lead To Up-Regulation of FTO, While the ALKBH5 Protein Level Was Stable During Aging but Up-Regulated During *in vitro*-Induced Cardiomyogenesis

Jana KREJČÍ[1], Orazio Angelo ARCIDIACONO[1], Radim ČEGAN[1], Katarzyna RADASZKIEWICZ[2], Jiří PACHERNÍK[2], Jan PIRK[3], Martin PEŠL[4], Petr FILA[5], Eva BÁRTOVÁ[1]

[1]Department of Cell Biology and Epigenetics, Institute of Biophysics, Academy of Sciences of the Czech Republic, Brno, Czech Republic, [2]Department of Experimental Biology, Faculty of Sciences, Masaryk University, Brno, Czech Republic, [3]IKEM, Cardiovascular Surgery Department, Prague, Czech Republic, [4]Department of Biology, Faculty of Medicine, Masaryk University, Brno, Czech Republic; International Clinical Research Center, St. Anne University Hospital, Brno, Czech Republic; 1st Department of Internal Medicine, Cardioangiology, St. Anne University Hospital and Faculty of Medicine, Masaryk University, Brno, Czech Republic, [5]Centre of Cardiovascular Surgery and Transplantation, Brno, Czech Republic; Department of Cardiovascular Surgery and Transplantation, Faculty of Medicine, Masaryk University, Brno, Czech Republic

Received February 7, 2023
Accepted May 25, 2023

Summary

FTO and ALKBH5 proteins are essential erasers of N^6-adenosine methylation in RNA. We studied how levels of FTO and ALKBH5 proteins changed during mouse embryonic development, aging, cardiomyogenesis, and neuroectodermal differentiation. We observed that aging in male and female mice was associated with FTO up-regulation in mouse hearts, brains, lungs, and kidneys, while the ALKBH5 level remained stable. FTO and ALKBH5 proteins were up-regulated during experimentally induced cardiomyogenesis, but the level of ALKBH5 protein was not changed when neuroectodermal differentiation was induced. HDAC1 depletion in mouse ES cells caused FTO down-regulation. In these cells, mRNA, carrying information from genes that regulate histone signature, RNA processing, and cell differentiation, was characterized by a reduced level of N^6-adenosine methylation in specific gene loci, primarily regulating cell differentiation into neuroectoderm. Together, when we compared both RNA demethylating proteins, the FTO protein level undergoes the most significant changes during cell differentiation and aging. Thus, we conclude that during aging and neuronal differentiation, m^6A RNA demethylation is likely regulated by the FTO protein but not *via* the function of ALKBH5.

Graphical Abstract

https://www.biomed.cas.cz/physiolres/graphabstract/935078.jpg

Key words

mES cells • hES cells • FTO • ALKBH5 • Epigenetics • Differentiation • Aging

Corresponding author

Eva Bártová, Department of Cell Biology and Epigenetics, Institute of Biophysics, Academy of Sciences of the Czech Republic, Brno, Czech Republic. E-mail: bartova@ibp.cz

Introduction

The physiological function within the epigenetic machinery leads to the accurate and fine-tuned execution of gene expression, cell fate programs, or cell stress response. Nowadays, the coordination and control of the post-transcriptional modification of the RNA are proving their essential role, raising the importance of epitranscriptomic regulation. The methylation on the N^6- position of adenosine (m^6A) has been known for almost 50 years [1-5]. It is the most abundant and functional modification of mRNA [6], but m^6A was also found in non-coding RNAs (ncRNAs) and long non-coding RNAs (lncRNAs) [7,8]. Moreover, among the over 100 chemically different modifications, in distinct

types of RNA have been discovered so far [9]. The methylation of RNA is conducted by a multiprotein complex composed of the heterodimer METTL3/ METTL14 (methyltransferase-like 3/methyltransferase-like 14) [10, 11] and the MACOM protein complex (m^6A-METTL-associated complex consists of WTAP, KIAA1429, RBM15, HAKAI, and ZC3H13) [11-14]. Also, additional RNA methyl transferase, METTL 16 (methyltransferase-like 16) installs m^6A in RNA [15,16]. To this fact, it is well-known that the m^6A mark on RNA is recognized by specific readers, such as the YTH (YT521-B) domain family proteins (YTHDF1, YTHDF2, YTHDF3, and YTHDC1) [17-21], or indirect readers, including the heterogeneous nuclear ribonucleoprotein HNRNPA2B1 and HNRNPC [22]. Besides specific readers, there is also the existence of specific m^6A erasers. In this case, the removal of the methyl group from N^6-adenosine is mediated by the FTO protein (fat-mass obesity-associated protein) [23] that oxidizes m^6A to N^6-hydroxymethyladenosine (hm^6A). Subsequently, the markers of active RNA demethylation, including N^6-formyladenosine (f^6A), and N^6-carboxyl-adenosine, appear [24]. Also, the ALKBH5 protein (alkB homolog 5) serves as an m^6A RNA eraser [25]. Due to the fact that the FTO protein regulates a number of physiological processes, the function of the FTO protein, its biological relevance, and its clinical significance have raised interest in the scientific community. Increasing evidence demonstrates that the FTO protein also plays a role in various cell differentiation processes. For example, it is involved in the control of adipogenesis through a dynamic m^6A RNA regulation that affects the splicing of a subset of genes [26]. *In vivo* study also showed the FTO role during myogenesis and the differentiation of the neuronal stem cells in adult mice [27, 28]. A relevant role of FTO is also emerging in cancer biology, where it is involved in the leukemogenesis process [29] or FTO inhibition leads to the suppression of cancer stem cell self-renewal and immune system evasion [30] or self-renewal of glioblastoma stem-cell neurospheres [31,32].

A fundamental role is also ascribed to m^6A RNA-mediated regulation of the translation process; thus, proteins essential for installation, maintenance, and removal of methylation from mRNA and tRNA are the focus of interest. For example, it was believed that m^6A is the preferred substrate for FTO, but Mauer and colleagues [33] showed that FTO preferentially demethylates m^6A_m (N6,2′-O-dimethyladenosine), an extended cap modification [33]. Mauer *et al.* [34] showed that FTO preferentially targets m^6Am residues in snRNAs, conversely to mRNAs. Thus, additional analyses showing the role of FTO targets are essential, especially from the view of the regulation of protein translation [35]. As it was published, the m^6A RNA level seems constant during mRNA life until its degradation [36,37]. The FTO protein does not demethylate the internal m^6A RNA in a sequence specific-manner (a hallmark of non-specific enzymatic activity). It acts at an unusually low rate reaction on it [5, 23, 38], while the demethylation rate is 100 times higher toward the cap m^6Am [33]. In this perspective, the observed internal m^6A-mRNA enrichment at 3' UTRs ends [39] may be explained by the increased activity of the FTO toward the m^6Am in the 5-cap structure [33]. A specific miCLIP analysis of the m^6A peak in wild-type and FTO-knockout mice revealed a subtle increase of m^6A at 5' UTR [46]. An additional miCLIP analysis of other RNA in FTO-knockout cells showed an increase of m^6Am in snRNA [34], accompanied by splicing defects [40]. These data suggest that the primary target of the FTO in the mRNA could be the m^6Am [33]. In this regard, the observation that the FTO seems to shuttle between the nucleus and the cytoplasm is also interesting from the view of its regulatory functions [41-43]. A recent study showed that the spatial localization of the FTO could influence its action on the target, where the FTO demethylates the internal m^6A RNAs in the nucleus and both the internal m^6A RNA and m^6Am during the mRNA capping [43].

Exciting is the clinical perspective of the m^6A RNA modification that seems to play an essential role in a common threat to cardiovascular disease (CVDs) [44-46]. For example, under ischemic stress, the FTO can selectively demethylate the cardiac contractile transcripts; and, therefore, increase their protein translation and finally improve the cardiac contractile function [46]. In neonatal rat cardiomyocytes, the hypertrophic effect of the adipokine leptin increased the nuclear FTO expression. At the same time, the FTO down-regulation suppressed the hypertrophic response, suggesting a role in cardiac physiology or pathology [47]. In a myocardial infarction model, the overexpression of FTO reduced cardiac fibrosis and enhanced angiogenesis [46]. An FTO-knockout mice model of heart failure (HF) showed a reduction in ejection fraction and enhanced dilatation, demonstrating the role of FTO in the faster progression of HF [48]. In addition, individuals with an FTO single nucleotide polymorphism (SNPs) indicate

a strong association with overweight/obesity due to reduced food satiety and increased food intake [49-52]. Also, it was demonstrated that FTO overexpression in mice could lead to obesity [53]. Generally, obesity is considered one of the main risk factors for CVDs [54, 55]. A study has demonstrated that inhibiting FTO *via* increasing the level of m^6A in RNA reduced the incidence of obesity and CVDs [56].

All these recent discoveries indicate an essential role of epitranscriptomic control, particularly for FTO and ALKBH5, as well, due to their m^6A RNA-demethylation activity in diverse biological processes. From this perspective, we studied the FTO and ALKBH5 expression profile in cardiac differentiation of mES cells during aging and after the intervention to the epigenome. In this case, we studied mES cells with HDAC1 (histone deacetylase 1) deficiency. Above mentioned data, and also as we showed in [57], decidedly indicate the fundamental role of FTO and ALKBH5 proteins in cardiomyogenesis. Moreover, the FTO protein regulates fat mass, thus, balancing human physiological body weight and obesity [58]. Also, it is known that the aging of human individuals is often associated with an increased body mass; thus, the knowledge of how FTO expression is changed during life span could shed light on the epigenetic regulation of aging. Also, based on FTO interaction networks [59], we studied the effect of HDAC1 depletion on the FTO protein level. For explanation, Shu Ran *et al.* [59] showed a functional interconnection between FTO and IFG1, which interaction network also includes HDAC1 and HDAC2. Moreover, Dong-feng Lu *et al.* [60, 61] suggested HDAC1 has a negative factor correlated with cardiac cell differentiation from mesenchymal stem cells. Thus, it makes sense that the study of both HDAC1 and FTO could contribute to a precise understanding of the molecular regulation of cardiomyogenesis.

Material and Methods

Cultivation and differentiation of mouse and human cell lines.

Undifferentiated mouse Embryonic Stem (mES) cells were routinely grown in Dulbecco's modified Eagle's medium (DMEM; #D6429, Sigma-Aldrich) supplemented with 15 % fetal calf serum (FCS; #16141-07, Gibco), non-essential amino acids (NEAA-100×, #11140-035, Gibco), 100 mM 1-thioglycerol (MTG; #M6145, Merck), 100 U/ml penicillin, and 100 µg/ml streptomycin (#XC-A4122, Biosera), and 1000 U/ml recombinant leukemia inhibitory factor (ESGROmLIF; #ESG1107, Millipore). We studied wild-type mouse embryonic stem cells, D3 line (HDAC1 wild-type, mES (wt)) [62], and mES cells that were deficient in HDAC1 (HDAC1 double null, mES (dn)) [63,64]. Mouse ES cells, HDAC1 (wt), were cultivated on 0.2 % gelatin-coated Petri dishes, and HDAC1 (dn) mES cells were grown on Matrigel-coated plastic dishes (#354277; Corning). *In-vitro* cell cultures were maintained at 37 °C in a humidified atmosphere containing 5 % CO_2.

The differentiation of mES cells into the cardiomyocytes was performed *via* embryoid bodies (EBs). EBs were created *via* the cultivation of mES cells in hanging drops, starting count of 300 cells/30 µl drop in complete ES media without adding LIF [65,66]. After 4 days of growing, EBs were transferred into bacteriological dishes and new ES media without LIF for additional two days. On the day of differentiation (dd) 6, the formed EBs were transferred onto tissue-culture gelatine-coated dishes for adhesion and propagation of differentiated cells with serum-free medium DMEM/F12 (#D8437, Sigma-Aldrich) supplemented with insulin, transferrin, selenium (ITS-100×; #41400-045, Gibco) and the medium was replaced every 2 days until the day of differentiation 20 (dd 20).

Neural differentiation in monolayer was induced by seeding mES cells into a culture medium without LIF. After 2 days, the cells were washed with PBS, and serum-free DMEM/F12 replaced the serum-containing medium supplemented with ITS (ITS-100×, #41400-045, Gibco), 2 µg/ml fibronectin (F; #F1141, Sigma-Aldrich), and 0.5 mM *all-trans* retinoic acid (ATRA; #R2625, Sigma-Aldrich) for additional 2 days and subsequently in DMEM/F12 medium with ITSF supplement alone. The medium was changed every 2 days until the day of differentiation 8 (dd 8) [67,68].

Cultivation and differentiation of human embryonic stem (hES) cells and induced human pluripotent stem (hiPS) cells

Human embryonic stem (hES) cell lines CCTL16 and CCTL17 were grown on Matrigel (#354277, Corning) coated dishes and were maintained in a commercial mTESR1 (#05850, StemCell technologies) culture medium. Differentiation was performed for five days using a STEMdif definitive endoderm kit (#05110, StemCell Technologies) according to the manufacturer's instructions. Human embryonic stem cells (line CCTL16

and CCTL17) were maintained according to the Czech national law Act. No. 227/2006 Coll and authorization of the human embryonic stem cell research No. MSMT-193036/2017-4.

Undifferentiated human induced pluripotent stem (hiPS) cells were cultured in iPSC medium (Essential 8 medium, #A15169-01, Gibco; 1x Essential supplement, #A15171-01, Gibco; 100U/ml Penicillin - 0,1mg/ml Streptomycin, #SV30010, Biotech) on vitronectin-coated (0.5 μg/ cm^2 rhVNT-N, #A14700, Gibco) standard tissue culture plastic. The medium was changed daily. Cells were passaged every 3-4 days when cells reached 70-85 % confluency. Before passage, standard tissue culture plastic was coated with 0.5 μg/cm^2 vitronectin diluted in Phosphate Buffer Saline (PBS) (137mM NaCl; 2.7mM KCl; 10mM Na_2HPO_4 • 2 H_2O; 10mM KH_2PO_4; pH 7.4) for one hour in 37 °C. The cells were washed twice with PBS; then incubated with 0.5mM EDTA (EDTA, Lachema) in PBS for 3-7 minutes at 37 °C. Subsequently, EDTA was gently removed and neutralized with 1 ml of iPSC medium. Cells were gently aspirated, and small clusters of cells were transferred into the new plate.

For differentiation, hiPS cells were replated on standard culture plastic coated for one hour at 37 °C with 0.017 mg/cm^2 growth factor reduced Matrigel (Matrigel-GFR, #356231, Corning) diluted in PBS. The medium was changed daily. When the iPS cells reached 90-95 % confluency, they were differentiated into cardiomyocytes (CMs) according to the standard cultivation protocol described by Lian *et al.* [69]. Briefly, cells were treated with 10μM CHIR99021 (#SML1046, Sigma) diluted in RPMI medium 1640 (#51800-019, Gibco), supplemented with 100 U/ml Penicillin and 0.1 mg/ml Streptomycin and 1x B27 insulin (#A18956-01, Gibco), here referred as RPMI/B27-INS. After 24 h, the medium was changed for fresh RPMI/B27-INS. Then 72 h after induction of differentiation, cells were treated with 5μM XAV939 (#X3004, Sigma), diluted in combined medium (1:1 mix of fresh RPMI/B27-INS with medium collected from the cultivation plate). The medium was changed after two days for fresh RPMI/B27-INS. On the seventh day, the RPMI/B27-INS cultivation medium was replaced by RPMI 1640 medium, supplemented with 100 U/ml penicillin and 0.1 mg/ml streptomycin and 1x B27 plus insulin (#17504-044, Gibco), here referred to as RPMI/B27+INS which was changed every other day from day 7. Beating cardiomyocytes were observed around day 10 of cell differentiation.

Experimental animals

All experimental animals were bred under protocols approved by the Branch Commission for Animal Welfare of the Ministry of Agriculture of the Czech Republic (permissions no. 91/2020). Mice line C57BL6 was obtained from the Breeding Facility of the Medical Faculty, Masaryk University, Brno, Czech Republic. The mice were housed in the Animal Core Facility of the Institute of Biophysics, the Czech Academy of Sciences, in a Specific Pathogen-Free (SPF) conditions, at 21-23 °C, in a 12 h light / 12 h dark cycle, and 50 % to 60 % relative humidity with *ad libitum* access to food and water. For experiments, embryos were used at the stage of embryonic development 13.5 (E13), 15.5. (E15), 18.8 (E18) days post conception (d.p.c.). Also, for studies, we used newborns, three-month-old mice (labeled as young animals), and 24-month-old mice (labeled as old animals).

Analysis of human heart samples

Human healthy and diseased heart atrial ad ventricular samples were obtained from post-transplantation cardiac patients diagnosed with dilated cardiomyopathy (DCM) or ischemic heart disease (IHD) that underwent ventricular assist device implantation or transplantation. All experiments were performed under the ethical standards of the Centre of Cardiovascular and Transplantation Surgery and approved by the Ethics Committee of the Centre of Cardiovascular Surgery and Transplantation, Brno, Czech Republic, and Department of Cardiovascular Surgery and Transplantation, Faculty of Medicine, Masaryk University, Brno, Czech Republic. The informed consent of all patients, attachment number 18, from Mar 18, 2020, is archived in the clinics. For the experiments, whole hearts, after explantation, were stored on ice, and within 25 minutes after induced fibrillation, were atrial and ventricular samples collected from visually healthy areas in the form of 1 cm blocks. These blocks were further divided into smaller sections and processed for subsequent analyses.

Western blot analysis

Western blot analyses were performed as previously described by [70]. We used the following primary antibodies: anti-FTO (#ab-92821, Abcam), anti-ALKBH5 (#a195377, Abcam), and secondary antibodies conjugated with horseradish peroxidase: anti-rabbit IgG (#AP307P, Sigma Aldrich), and anti-mouse IgG

(#A9044, Sigma-Aldrich). The quantification of protein levels was processed by ImageJ software. Relative density values of western blot fragments of each protein were compared to the relative density of the total protein levels. In all blots, the ratios of all samples were normalized to the ratio measured in mES HDAC1 (wt) cells. This parameter was assigned a value of 1 in each quantification chart.

Embryonic tissue cryo-sectioning and immunohisto-chemistry

After explantation of organs from embryos, the embryonic hearts and brains were fixed with 4 % formaldehyde (FA; #AAJ19943K2, Thermo Fisher Scientific) overnight at 4 °C, after washing three times for 30 minutes in cold PBS, tissues were cryo-protected by 30 % sucrose in PBS (changed three times/ 12 hours) at 4 °C. Next, the cryoprotected embryonic organs were transferred to embedding matrix OCT (Leica Microsystems) and moved into the moulds containing OCT, and froze to -20 °C. The tissues were sectioned using a LeicaCryo-Microtome (LeicaCM1800, Leica). Deeply frozen samples were cut into a section of 14 µm thickness.

Immunostaining of tissue sections was started by re-fixation of sections plated on microscope slides in 4 % FA. Samples were washed in PBS, and permeabilization was done by 1 % Triton X-100 in PBS (8 min, RT) and saponin solution (0.1 % saponin, 0.1 % Triton X-100 in PBS; the treatment was for 12 min, RT) was used. Undifferentiated mES cells, cultured on microscopic culture dishes (#80158, Ibidi) with appropriate coating, were fixed by 4 % FA. After washing, the permeabilization was conducted with 0.1 % Triton X- in PBS (8 min, RT) and saponin solution (0.1 % saponin, 0.1 % Triton X-100 in PBS, the treatment for 12 min, RT). A blocking solution of 1 % bovine serum albumin (BSA; #A2153-506, Sigma Aldrich) in PBS was used for one hour at RT. For staining of both (tissue sections and cells), the following antibodies were used: anti-FTO (#ab-92821, Abcam); anti-ALKBH5 (#a195377, Abcam), and secondary antibodies Alexa Fluor 488 anti-rabbit IgG (#ab150077, Abcam); Alexa Fluor 594 anti-mouse IgG (#A11032, ThermoFisher Scientific). The nuclear DNA was stained by 4',6-diamidino-2-phenylindole (DAPI; #10236276001, Merck Life Science), and objects were mounted into Vectashield Mounting Medium (#H-1000, Vector Laboratories).

Confocal and tile-scanning microscopy

Fluorescence images were acquired by a confocal microscope (TCS SP8 SMD, Leica Microsystems, Germany) equipped with white light laser (WLL) and 405 nm laser, a motorized *x-y* stage, hybrid (HyD) or photomultiplier (PMTs) detectors. We used objectives: HC PL APO CS2 63x Oil, NA 1.4, WD 0.14 mm, and HC PL APO CS 10x, NA 0.40, WD 2.2 mm (Leica Microsystems). Image acquisition was performed using LAS X software (Leica Microsystems, Germany). Stacks of confocal images were collected automatically at *z*-distances steps 0.3 µm for mES cells and 1 µm for tissue sections. Image acquisition was performed at a resolution of 1024 × 1024 pixels, 400 Hz, zoom 1, and images were presented as maximum intensity projections. Tissue sections were captured using the tile-scanning mode. Acquired panels were auto-stitched in smooth mode, and the image reconstruction was performed by LAS X software (Leica Microsystems). Quantification of fluorescence intensity was performed by Leica LAS X software, according to selected regions of interest (ROIs) highlighted in images obtained by confocal microscopy and immune-fluorescence.

Embryos and embryonic hearts were visualized by a 3D digital microscope Keyence VHX-7000; 4K camera equipped by sensor CMOS 1/1.7 inch; 12.22 megapixels; objective E20 magnification 20× (KEYENCE INTERNATIONAL).

RIP-Seq analysis

The HDAC1 (wt) and HDAC1 (dn) mES cells in the undifferentiated stage (labelled as wtC, dnC) and mES cells induced to neuro-ectodermal differentiation for 8 days (labelled wtDif, dnDif) were examined by RNA immunoprecipitation, combined with sequencing analysis (RIP-Seq). RNA isolation was performed by Gen Elute Universal Total RNA purification kit (#RNB100, Sigma Aldrich), and 50 ng of RNA was used for the library preparation. We used the Magna RIP RNA-Binding Protein Immunoprecipitation Kit (#17-700, Millipore). An antibody of interest was anti-m^{6}A RNA (#202 111, SYSY Antibodies). Sequencing libraries were prepared by Lexogen QuantSeq FWD SR75 library preparation kit, used for Illumina sequencing (Lexogen). The sequencing of the libraries was conducted on Illumina NextSeq (Illumina Inc.) instrument with 75 bp single-end reads. The quality of sequencing reads was inspected in FastQC (https://www.bioinformatics.babraham.ac.uk/projects/fastqc). Read trimming on quality (Q30) and sequencing adaptor removal were done with Trimmomatic -0.32 [71]. Cleaned reads from each library were mapped onto the *Mus musculus* (GCA_000001635.9_GRCm39_

genomic.fasta; GCF_000001635.27_GRCm39_genomic .gtf) reference genome using STAR aligner v 2.2.7a. STAR: ultrafast universal RNA-seq aligner [72]. Mapped reads quantification was done by package subread 1.5.2 - featureCounts [73] and were used as input for differential peak analysis using the Bioconductor package MeTDiff (version 1.1.0; [74]). The peaks were considered differentially expressed in each comparison when the false discovery rate was <0.05 (Supplementary Table S2). The Venn diagram was created by an online tool available at https://bioinformatics.psb.ugent.be/webtools/Venn/. The upset plot was done by the R package UpSetR (version 1.4.0; [75]).

Data statistical analysis

The following programs were used: Leica LAS X software (Leica Microsystems), ImageJ software (see www. imagej.nih.gov, NIH USA freeware), and SigmaPlot software (version 13.0, Systat). With Sigma Plot software, we evaluated our data using paired Student's t-test, and p-values ≤ 0.05 were considered statistically significant. Statistically significant differences from control values are shown using asterisks (red asterisks indicate increased protein levels and blue asterisks show decreased protein levels).

Results

Our study used an *in vitro* differentiation model of mES cells, established on the embryoid body formation [76], which closely resembles the embryonic development of all three germ layers, including the cardiomyocytes [62,77]. Using the model described in our previous study, we analyzed the more profound role of FTO and ALKBH5 proteins during differentiation processes. We studied changes in described protein levels during development and aging in experimental mouse models. Also, we studied the FTO and ALKBH5 protein levels in mouse embryonic and adult hearts, brains, lungs, and kidneys, as well as human hearts obtained after heart transplantation. Considering the emerging evidence of crosstalk between the m^6A RNA and other epigenetic regulators [78], we attempted to address if there is a connection between histone regulation, especially regulation of histone acetylation, and changes in the m^6A RNA level.

Canges in the level of FTO and ALKBH5 during mouse embryonic development

We studied changes in the level of the FTO and ALKBH5 proteins in mouse embryonic hearts and brains at developmental stages E13, E15, and E18 (Fig. 1A, B). Using immunofluorescence and tile scanning, we observed that FTO and ALKBH5 proteins occupy the cortex of E15 brains (Fig. 1C). Figure 1D shows the maximum concentration of proteins in the parts of the interatrial septum where the most common congenital heart defect occurs. In most human cases, there is a defect of the interatrial septum in the septum secundum or foramen ovale anatomical part. Anatomical parts were determined according to [79].

Performing western blots, we observed the highest FTO level in E13 brains compared to E13 hearts and mouse embryonic stem (mES) cells. The FTO level was identical in E13, E15, and E18 hearts, but we observed FTO down-regulation during mouse brain development (compare E13 and E18 stages in Fig. 1E and Fa). The level of the ALKBH5 protein was significantly lower in embryonic hearts and brains when compared with mES cells. Notably, the ALKBH5 level was reduced during the development of mouse hearts and brains at the E18 stage and in newborn animals (Fig. 1Fb).

Changes in the level of FTO and ALKBH5 during aging

Western blots showed an increased level of the FTO protein in the aortas, atria, and ventricles of old male animals compared with young males (Fig. 2Aa,b). The ALKBH5 protein was barely detectable in adult mouse hearts compared to mES cells (Fig. 1Ac). We also studied FTO and ALKBH5 protein levels in mouse brains, and we observed the highest level of the FTO protein in olfactory bulbs of old animals of both genders compared to young individuals (Fig. 2Ba,b). The ALKBH5 level was relatively low in mouse brains compared to mES cells but the highest in olfactory bulbs of young and old animals compared with hippocampi and cortex (Fig. 2Ba, c). Also, we studied FTO and ALKBH5 protein levels in the lungs and kidneys of young and old mice. In the lungs of young males, we observed the lowest level of FTO compared to old animals. Especially old male mice were characterized by a very high level of FTO in their lungs (Fig. 2Ca, b). Again, the ALKBH5 level was very low in studied tissues compared to the ALKBH5 level in mES cells (Fig. 2Ca, c). In mouse kidneys, we observed FTO up-regulation in especially old males. The ALKBH5 protein was again barely detectable when comparing the ALKBH5 level in mouse kidneys with the ALKBH5 pool in mES cells (Fig. 2Da-c).

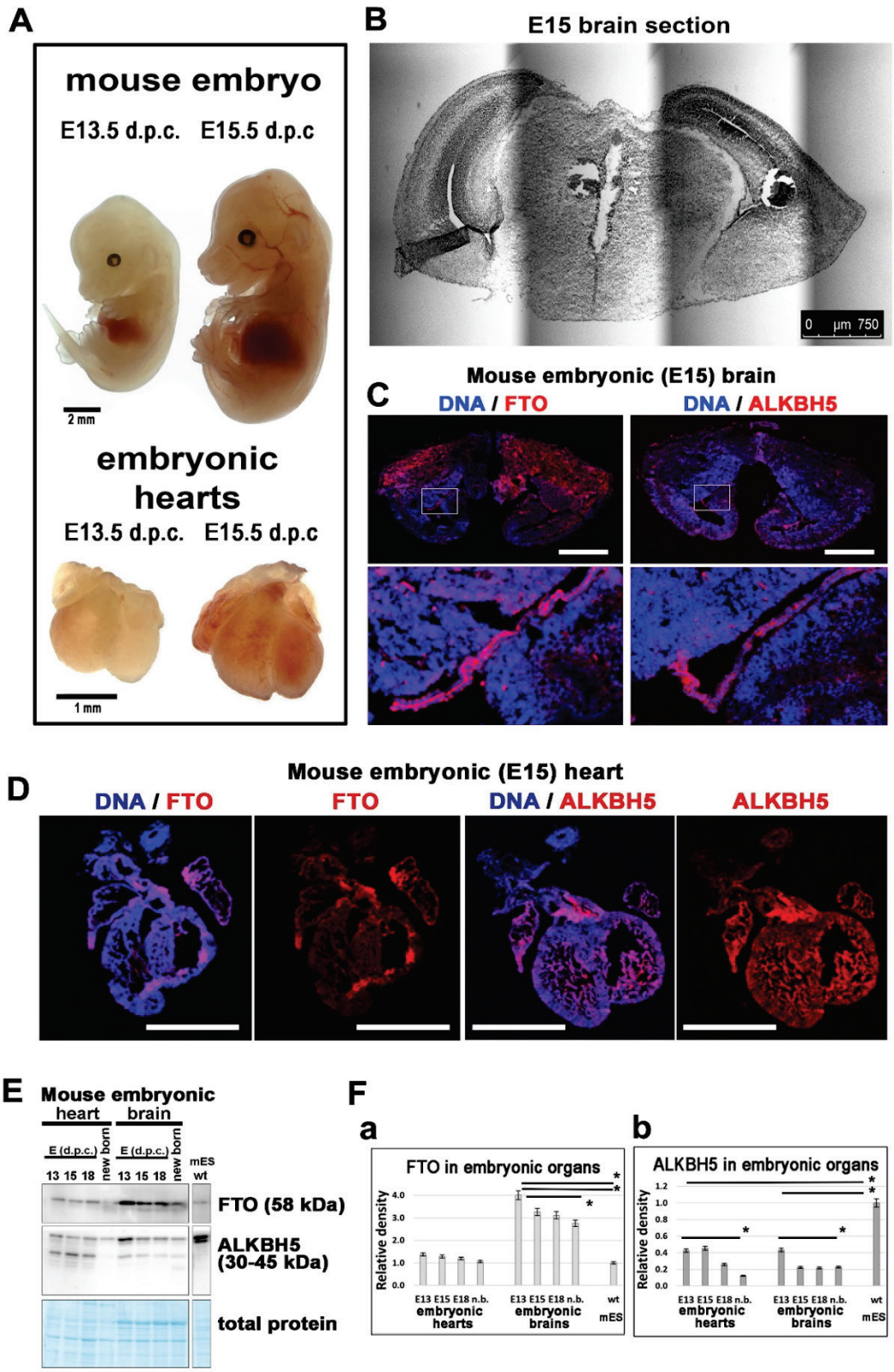

Fig. 1. The FTO and ALKBH5 levels during mouse embryonic development. **(A)** Mouse embryo E13 or E15, and E13 or E15 embryonic hearts. **(B)** Tile scanning of e15 mouse brain. **(C)** Tile scans showed FTO and ALKBH5 localization in mouse E15 embryonic brains. White frames in the upper panels show the brain cortex magnified in the lower panels. Scale bar shows 1 mm. **(D)** FTO and ALKBH5 proteins were visualized in mouse heart sections from E15 embryonic hearts. Immunofluorescence and tile scanning was used for this analysis. Scale bar shows 1 mm. **(E)** Western blot analysis of the FTO and ALKBH5 levels in E13, E15, and E18 embryonic hearts and brains. Data were normalized to the total protein levels and quantified by ImageJ software showing the level of **(Fa)** FTO and **(Fb)** ALKBH5. Data were compared with the level of FTO, and ALKBH5 was analyzed in mES cells. Asterisks in panel F show statistically different results at $p \leq 0.05$.

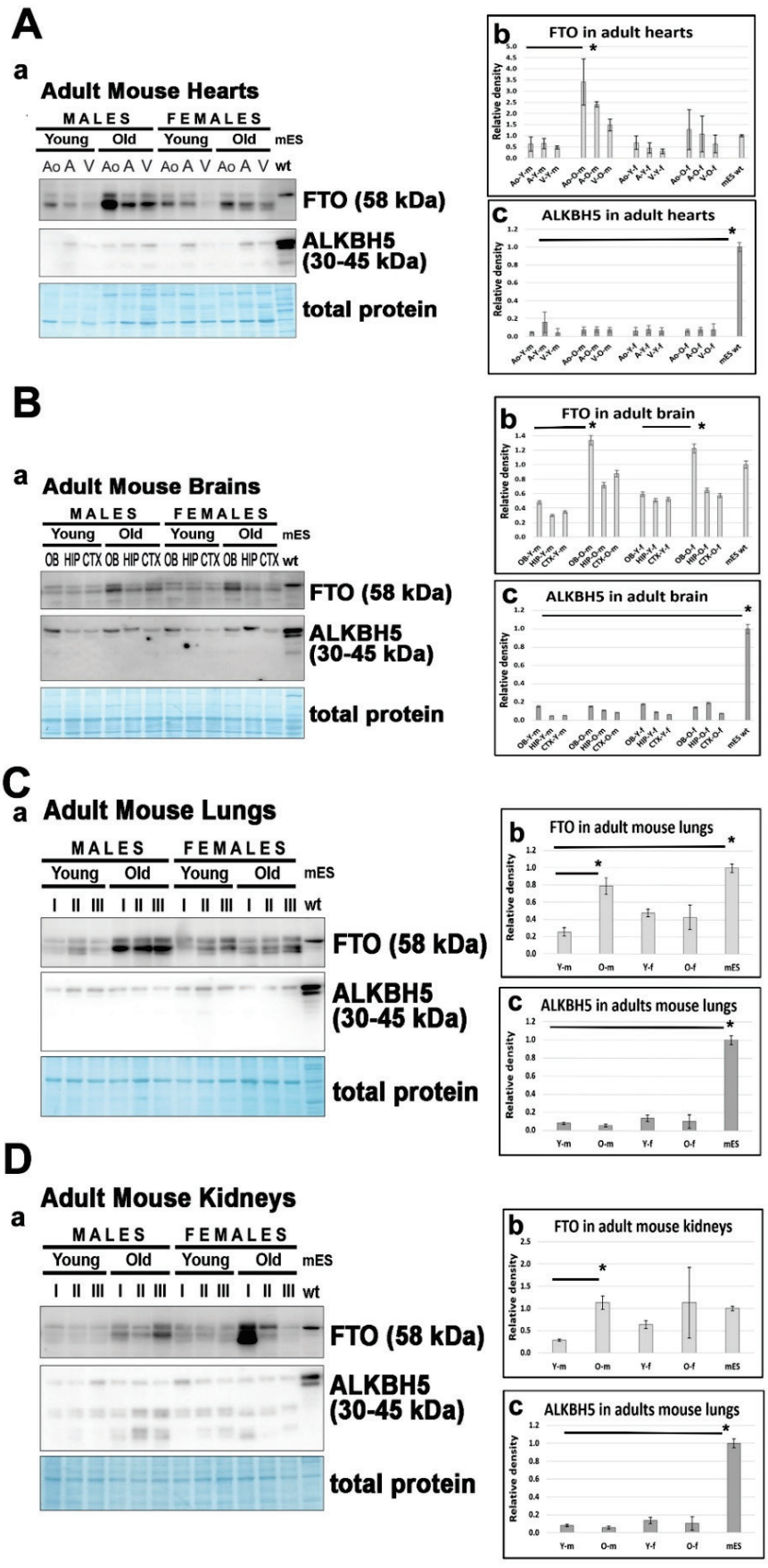

Fig. 2. Changes in the FTO and ALKBH5 levels in mouse hearts, brains, lungs and kidneys during aging. The FTO and ALKBH5 protein levels were studied in young (Y) and old (O) adult **(Aa)** hearts – aorta (Ao), atrium (A), ventriculus (V), **(Ba)** brains – olfactory bulb (OB), hippocampus (HIP), cortex (CTX), **(Ca)** lungs, and **(Da)** kidneys in male (m) and female (f) animals compared to mES cells. Data are compared to the total protein levels and quantified by the ImageJ software. The normalized levels of the FTO protein are shown in both panels **b**, and the ALKBH5 proteins are normalized levels in panels **c**. Asterisks show statistically different results from the control values at $p \leq 0.05$.

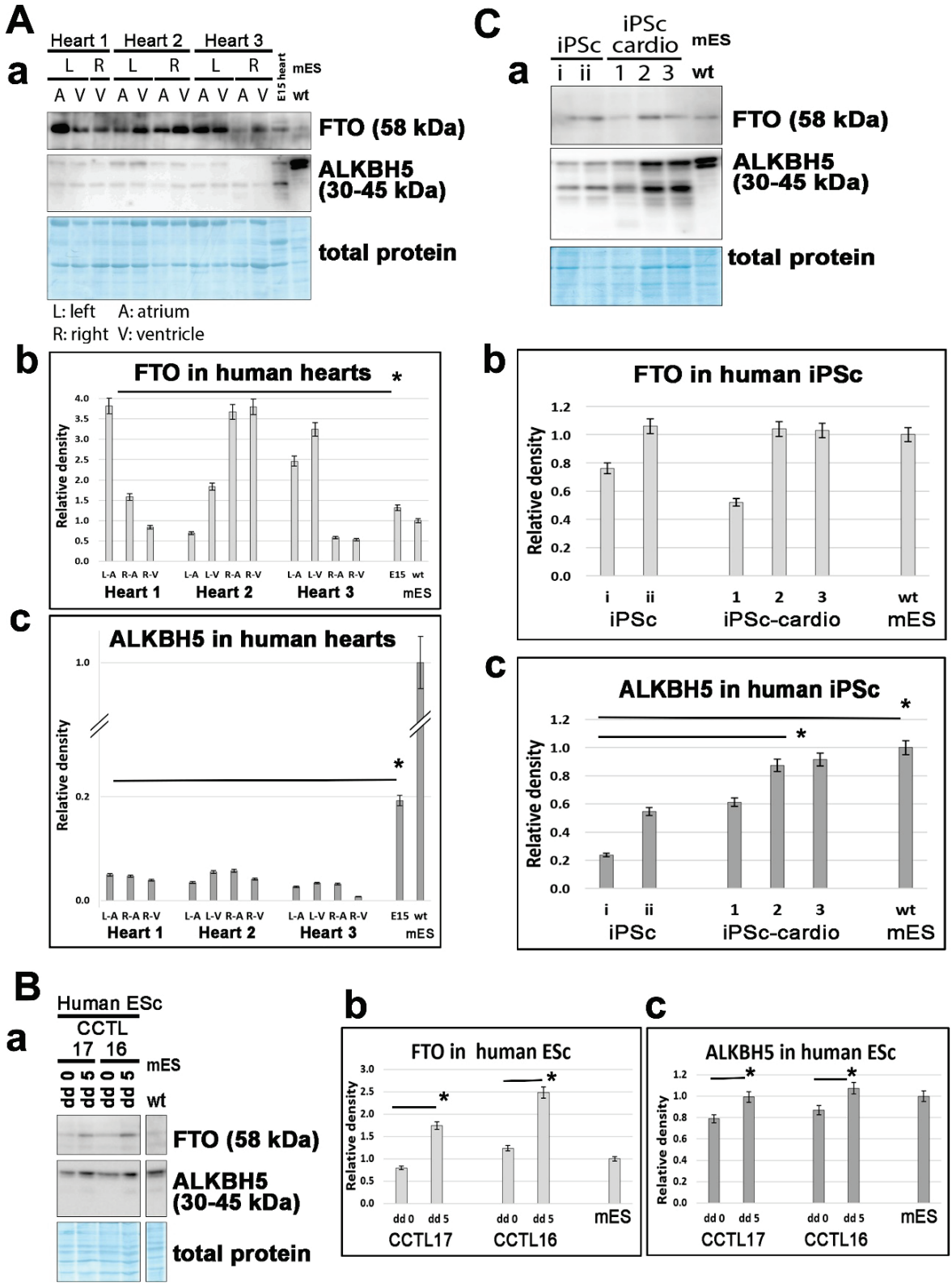

Fig. 3. The level of FTO and ALKBH5 proteins in human hearts hES cells and hiPS cells induced into cardiomyogenesis. Western blot studies were performed in **(A)** human hearts, **(B)** hES cells, and **(C)** hiPS cells induced into cardiomyogenesis. **(Aa-c)** Differences in the FTO level were observed in the atria and ventriculi of human hearts compared to mES cells. The level of the ALKBH5 protein was relatively low. Western blot data were normalized to the total protein levels. **(Ba-c)** The level of FTO and ALKBH5 in hES cells normalized to the total protein levels and compared with mES cells. Asterisks show statistically different results at $p \leq 0.05$. **(Ca-c)** The level of FTO and ALKBH5 in hiPS cells normalized to the total protein levels and compared with mES cells. The asterisks show statistically different results at $p \leq 0.05$.

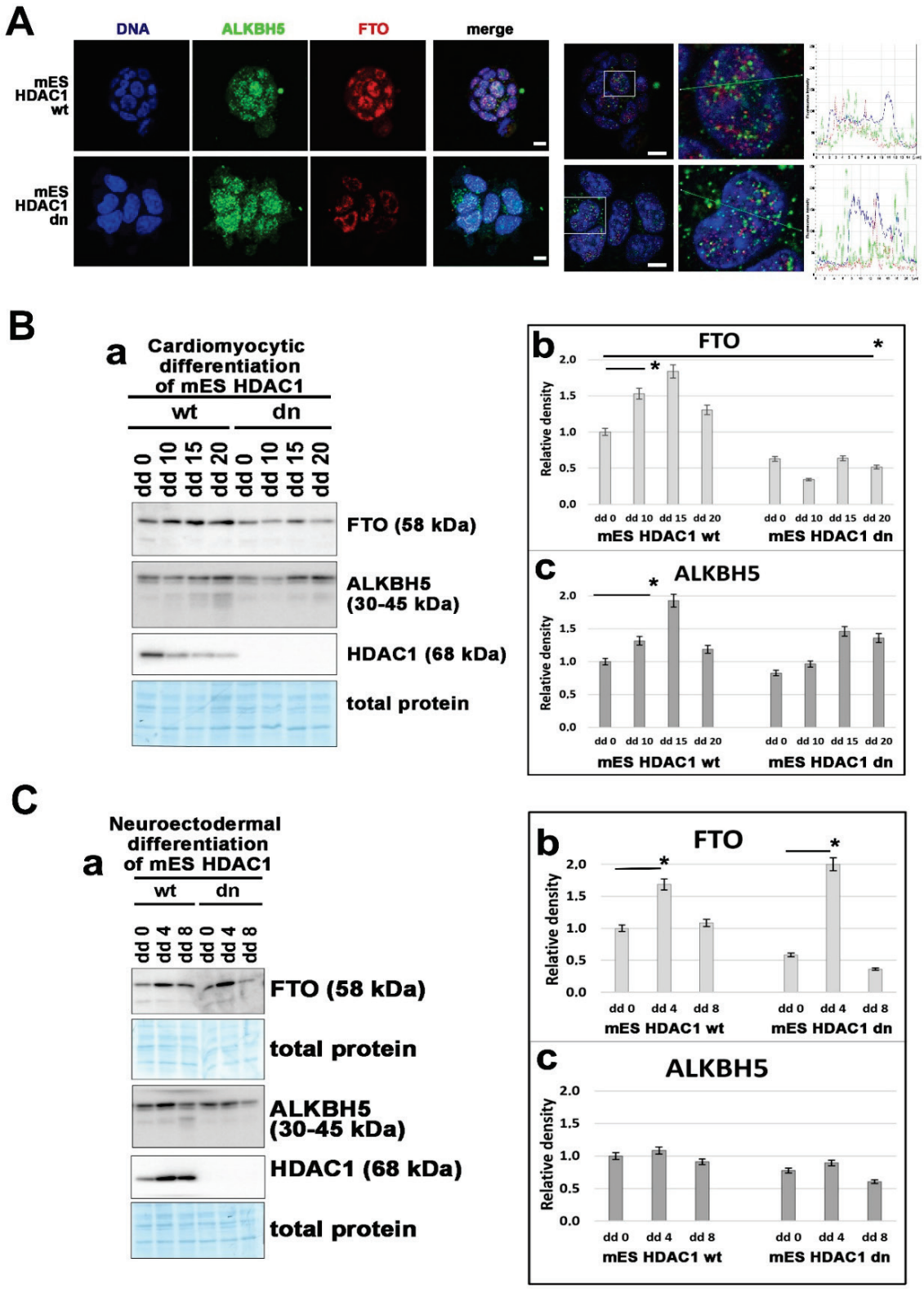

Fig. 4. The levels of FTO and ALKBH5 protein levels were studied in wild-type mES cells and HDAC1 (dn) mES cells. **(A)** Immunofluorescence and confocal microscopy showed the localization of FTO and ALKBH5 proteins in non-differentiated HDAC1 (wt) and HDAC1 (dn) mES cells. Quantification of the fluorescent intensity was performed by the Leica LAS X software. Scale bars show 20 μm. **(Ba-c)** Cardiomyocytic differentiation of mES. Western blots showed FTO down-regulation in HDAC1-depleted cells, while the ALKBH5 level was identical in (wt) and HDAC1 (dn) cells. In (wt) mESs, differentiation into cardiomyocytes caused up-regulation of both FTO and ALKBH5 proteins. **(Ca-c)** Neuroectodermal differentiation of mES. In HDAC1 (wt) and HDAC1 (dn) mES cells, the 4th day of differentiation (dd 4) into neuroectoderm was characterized by FTO up-regulation. At the same time, the level of ALKBH5 remained stable during experimentally induced differentiation in the neuroectoderm. Data from panels B and C were normalized to the protein level and quantified by ImageJ software. The asterisks show statistically different results from the control values at $p \leq 0.05$.

Analysis of the level of FTO and ALKBH5 proteins in human hearts in pathophysiological state

Compared to E15 mouse hearts and mES cells, we found a relatively high level of the FTO protein in human hearts. The level of FTO varies among the atria and ventriculi of individuals studied (Fig. 3Aa,b). The ALKBH5 level in human hearts was very low compared to mES cells and E15 mouse embryonic brains (Fig. 3Ac). When compared with pluripotent human embryonic stem cells (hES cells, lines CCTL16, and CCTL17) and mES cells, differentiated hES cells into endoderm were characterized by FTO up-regulation confirmed the existence of the FTO up-regulation during human cardiomyogenesis (Fig. 3Aa, b and Ba, b). Also, during the differentiation of hES cells into cardiomyocytes, the ALKBH5 was up-regulated, but the level of ALKBH5 was identical in both pluripotent hES and mES cells (Fig. 3Ba,c).

Also, we studied FTO and ALKBH5 proteins in human-induced pluripotent stem cells (hiPS cells), in which we induced cardiomyocytic differentiation. In this case, cardiomyogenesis was not accompanied by changes in the FTO level, but ALKBH5 was significantly up-regulated (Fig. 3Ca-c). In addition, mES cells were characterized by a higher ALKBH5 level than hiPS cells (Fig. 3Ca,c).

The FTO protein was down-regulated in HDAC1-depleted mouse embryonic stem cells and up-regulated during experimentally induced cardiomyogenesis in wild-type mES cells.

We studied the nuclear distribution of FTO and ALKBH5 proteins in wild type (wt) and HDAC1 double null (dn) mouse embryonic stem (mES) cells, and these cells were induced toward cardiomyogenesis (Fig. 4A). We observed that HDAC1 deficiency does not affect the distribution of FTO and ALKBH5 proteins inside the cell nucleus. Notably, both proteins were localized in the nucleoplasm, and the ALKBH5 protein also occupied the cytoplasm. We observed that the FTO protein is localized in only the nucleoplasm (see quantification of the fluorescence intensity in panels 4A).

In the following experiments, we studied pools of FTO and ALKBH5 proteins during experimentally induced cardiomyogenesis. On day 15 of differentiation, western blots showed up-regulation of the FTO protein level when we analyzed cardiomyogenesis in HDAC1 (wt) mES. Importantly, HDAC1 depletion caused significant down-regulation of FTO (see HDAC1 (dn) mES cells in Fig. 4Ba,b). The ALKBH5 protein was up-regulated in HDAC1 (wt) mES cells and cardiomyocytes, studied on the 15th day after induced differentiation (Fig. 4Ba,c).

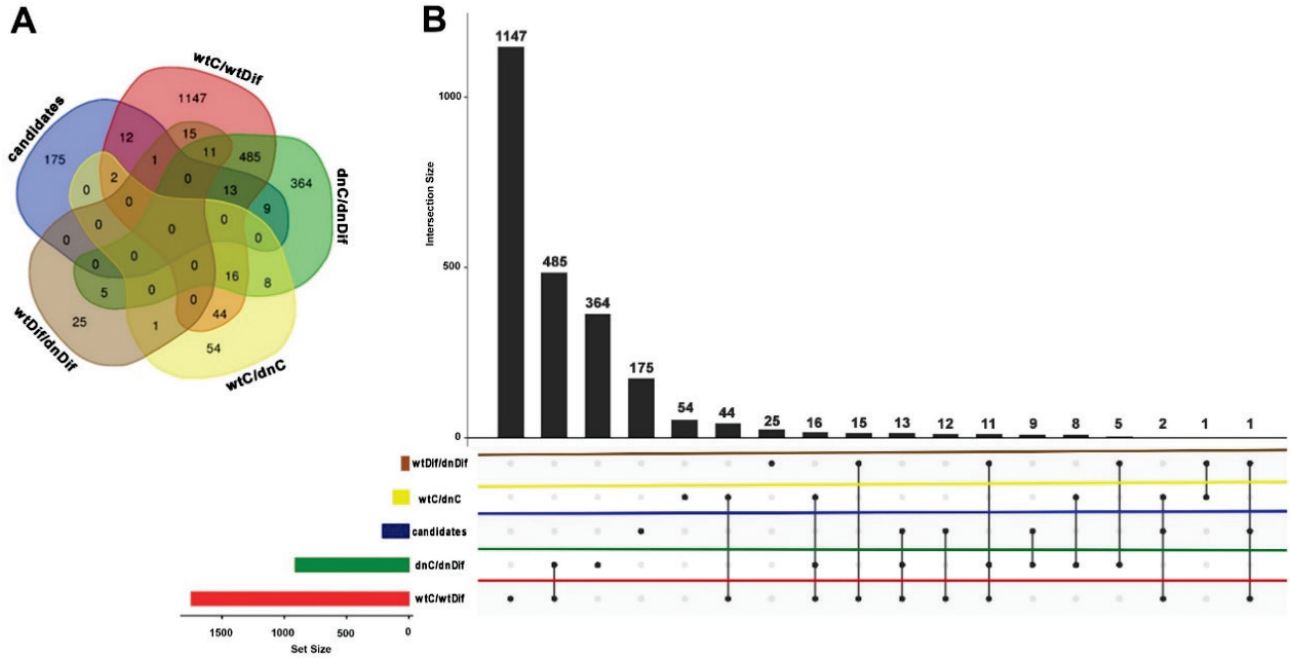

Fig. 5. Venn diagram and Upset plot of intersections between sets of differential m^{6}A peaks in (wt) and (dn) conditions and candidates genes. **(A)** Venn diagram shows the total number of genes with differentially expressed m^{6}A peaks for mRNA encoded by candidate genes. **(B)** The bar chart indicates the intersection size between sets of genes. Black connected dots on the bottom panel indicate which sets of genes are considered for each intersection.

Table 1. Overview of 212 candidate genes that were targeted by RIPseq data analysis

Cellular process	Candidate genes
Histone code regulation	*Hdac1 Hdac2 Hdac3 Hdac5 Hdac7 Hdac8 Hdac9 Hdac10 Hdac11 Suv39h1 Hat1 Jmjd6 Jmjd1c Jmjd4 Jmjd8 Kdm1a Kdm1a Kdm6b Kdm3b Kdm4b Kdm6a Kdm4c Kdm2b Kdm1b Kdm7a Kdm8 Kdm5d Kat5 Kat6a*
RNA processing	*Mettl2 Mettl3 Mettl4 Mettl5 Mettl7a1 Mettl8 Mettl14 Mettl15 Mettl17 Mettl21a Mettl21e Mettl22 Mettl23 Mettl25 Mettl27 Alkbh5 Pcif1 Zc3h13 Foxm1 Ezh2*
Stemness and Embryonic Development	*Sox1 Sox2ot Sox3 Sox5 Sox6 Sox7 Sox8 Sox9 Sox10 Sox11 Sox13 Sox14 Sox17 Sox18 Sox21 Sox30 Qsox1 Qsox2 Sox1ot Sox5os3 Sox5os4 Sox6os Pou1f1 Pou2af1 Pou2f1 Pou2f2 Pou2f3 Pou3f1 Pou3f2 Pou3f3 Pou3f4 Pou4f1 Pou4f2 Pou4f3 Pou5f1-rs1 Pou5f1-rs4 Pou5f1-rs6 Pou5f1-rs8 Pou5f2 Pou6f1 Pou6f2*
Neuroectoderm differentiation	*Neurod1 Neurod2 Neurod4 Neurod6 Neurog1 Neurog2 Neurog3 Gfap Ncam1 Ncam2 Ntf3 Ntf5 Tubb3 Myt1l Sema3a Rpl10a Brinp1 Hpcal1 Nedd4 Nedd8 Nedd9 Anxa6 Coro1c*
Cardiogenesis	*Tpm1 Tnnt2 Myh10 Nppa Foxc1 Dkk1 Isl1 Islr Nkx2-5 Nkx2-4 Nkx6-3 Nkx2-9 Tbx5 Tbx20 Gata4 Gata6 Gata3 Gata2 Gata1 Gata5 Mef2c Mef2a Mef2c Mef2d Hand1 Hand2 Myh6 Myh7 Myh7b Rpl13a Myl2 Myl7 Mesp1 Mesp2*
Cell signaling	*Stat3 Socs3 Jak2 Jak1 Jak3 Notch1 Notch2 Notch3 Notch4 Hes1 Hes2 Hes3 Hes5 Hes6 Hes7 Akt2 Akt3 Wnt2b Wnt3a Wnt3 Wnt4 Wnt5a Wnt5b Wnt7a Wnt7b Wnt8a Wnt8b Wnt9a Wnt9b Wnt10a Wnt10b Wnt11 Wnt16*

Interestingly, FTO was up-regulated on the 4th day of differentiation into neuroectoderm, induced in both HDAC1 (wt) and HDAC1 (dn) mES cells. However, the level of the ALKBH5 protein remained relatively stable in this differentiation pathway, induced experimentally (Fig. 4Ca,c).

The density of m^{6}A RNA modification in non-differentiated and differentiated wild-type and HDAC1 deficient ES cells.

The HDAC1 (wt) and HDAC1 (dn) cells were induced into neuro-ectodermal differentiation for eight days. In this case, we performed RIP-Seq analysis to see the distribution of RNAs methylated on N^6-adenosine (m^{6}A RNA) preferentially in 3´-UTR [80] (Supplement S1). In a group of analyzed genes encoding m^{6}A mRNA, we focused on loci associated with epigenetic regulation, features of epitranscriptome as well as cell differentiation (Fig. 5A, B and Supplement S2). Supplementary files S1 and S2 are available at the URL: https://www.ibp.cz/en/research/departments/cellular-biology-and-epigenetics/open-data/krejci-et-al-2023. By the use of RIP-Seq analysis, we observed that 1147 genes were unique when comparing HDAC1 (wt) control (non-differentiated) mES cells and differentiated cell population (wtC/wtDif). During neuroectodermal differentiation, in both mES cell lines, the abundance of m^{6}A mRNA was changed in 485 genetic elements. Notably, in this case, the HDAC1 status does not influence the methylation of RNA. The methylated mRNA of 364 genes was unique when comparing HDAC1 (dn) non-differentiated mES cells and their differentiated counterpart (dnC/dnDif) (Fig. 5A, B).

When analyzing undifferentiated HDAC1 (wt) and undifferentiated HDAC1 (dn) mES cells (wtC/dnC), we detected 54 unique genes in which methylated RNA was changed (Fig 5A,B). When comparing differentiated mES cells (wt) and HDAC1 (dn) cells (wtDif/dnDif), we found 25 genes, of which mRNA was modified on m^{6}A (Fig. 5A,B). In detail, RIP-Seq analysis was focused on the candidate genes. The overview of the candidate genes is shown in Table 1, listing 212 genetic elements. Candidate genes were selected according to their function in cellular processes. We were interested in histone code regulation, RNA processing, stemness and embryonic development, neuroectodermal differentiation, cardio-myogenesis, and cell signaling). For example, in these 175 loci, we did not detect changes in m^{6}A RNA content; see the blue field in Fig. 5A and the dot in the blue line of Fig. 5B. We have additionally observed that differentiation of HDAC1 (wt) mES cells into neuroectoderm was accompanied by loss of m^{6}A marker in mRNA of 28 candidate genes (wtC/wtDif); 19 candidate genes was characterized by depletion (loss) of m^{6}A methylation in HDAC1 (dn) mES cells induced to neuroectoderm (dnC/dnDif). Above mentioned candidate

Table 2. Changes of m^{6}A mRNA level studied during neuroectodermal differentiation of HDAC1 (wt) and HDAC1 (dn) mES cells by RIP-Seq analysis

Cellular process	Genes	wtC/wtDif	dnC/dnDif	wtC/dnC	wtDif/dnDif	Function
Regulation of histone code	Hdac4	loss				histone deacetylase
	Hdac6	loss				histone deacetylase
	Kdm2a	loss		loss		lysine demethylase
	Kdm3a	loss				lysine demethylase
	Kdm5a	loss				lysine demethylase
	Kdm5b	loss	loss			lysine demethylase
	Kdm5c	loss	loss			lysine demethylase
	Kat2a	loss				lysine acetytransferase
	Kat6b	loss	loss			lysine acetytransferase
	Ep300	loss	loss			histone acetyltransferase
	Jmjd7	loss	loss			arginine/lysine demethylase
RNA processing	Mettl1		loss			methyltransferase of N(7)-methylguanosine in RNA
	Mettl6	loss	loss			tRNA m3C methyltransferase
	Mettl9		loss			protein-L-histidine N-pros-methyltransferase
	Mettl16	loss				RNA N6-methyltransferase
	Mettl18	loss	loss			histidine-specific methyltransferase
	Mettl26	loss				methlytransferase with unknown function
	Mettl27	loss				ubiE/COQ5 methyltransferase family
	Fto	loss				RNA m6A-demethylase
	Wtap	loss	loss			in m6A methyltransferase complex function
	Virma	loss	loss			mRNA polyadenylation and mRNA methylation
	Rbm15		loss			regulator of m6A methylation of RNAs
	Rbm15b	loss	loss			regulator of m6A methylation of RNAs
	Dcp2		loss			mRNA-decapping complex/mRNAs degradation
Stemness/embryonic development	Nanog	loss	loss			the self-renewal of embryonic stem cells
	Sox2	loss		loss		regulation of pluripotency and neural differentiation
	Sox4	loss			gain	regulation of embryonic development
	Sox12		loss			regulation of embryonic development
	Sox15	loss				regulation of embryonic development
Neuroectoderm dif.	Rest	loss	loss			repression of neural genes in non-neuronal cells
Cardiomyogenesis	Actn1		gain			F-actin cross-linking protein
	Arvcf	loss				role in the formalin of adherens junction complexes
Cell signaling	Akt1		gain			involve the binding of membrane-bound ligands
	Jak1	loss				tyrosine kinase protein of INF-transduction pathway
	Hes6	loss	loss			promotes cell differentiation
	Wnt6		gain			embryonic structures formation and maturation
	Wnt7b		loss			regulation of cell fate and patterning during embryogenesis

Table 2 specifies the results shown in Fig. 5A, and colorized loss/gain in the table correspond to the color of intersections of studied subsets of genes in Fig. 5A. The table shows the listed names of genes of which m^{6}A mRNA modification underwent changes caused by cell differentiation or by HDAC1 depletion. [Abbreviations: (wt): HDAC1 wild type mES cells; (dn): double null HDAC1 mES cells; C: control/undifferentiated cells; Dif: cells differentiated into neuroectoderm].

genes and changes in their methylated mRNA are listed in Table 2, showing the loss (depletion) and gain (upregulation) of m^{6}A mRNA. RIP-Seq analysis additionally showed that *Actn1, Akt1,* and *Wnt6* genes were an exception; see m^{6}A RNA increased level in differentiated HDAC1 (dn) cells (Table 2, Supplement S1 and Supplement S2). Moreover, 12 genes were unique for m^{6}A methylation of their mRNA when studied in

differentiated HDAC1 (wt) mES cells (wtC/wtDif, see exclusively red frames in Table 2, which correspond to the pink intersection between blue and red color in Fig. 5A). One of them was the *Fto* gene, of which mRNA also lost the m^6A-modification mark during the differentiation of HDAC1 (wt). Still, it was not the case for HDAC1 (dn) cells. Also, methylation of mRNA encoded by *Kdm2a* and *Sox2* genes was reduced not only during the differentiation of (wt) mES (wtC/wtDiff) cells but also the same trend we observed in HDAC1 (dn) cells (Table 2). Interestingly, 9 unique genes were characterized by changes (preferentially depletion) in m^6A RNA studied during neuroectodermal differentiation of HDAC1 (dn) cells (see exclusively green frames in Table 2 and the intersection of the blue and green fields shown in Fig. 5A). Both (wt) and (dn) mES cell lines were characterized by reduced m^6A RNA levels in 13 genes when studied during differentiation (see the combination of red and green frames in Table 2, and the intersection between blue, red and green subsets of genes shown in Fig. 5A and 5B). Also, we compared control non-differentiated (wt) and (dn) mES cells (wtC/dnC), and in this case, there was a loss of m^6A in mRNA encoded by the *Kdm2a* gene and the *Sox2* gene (see exclusively yellow frames in Table 2 and two genes in the intersection of the blue, red and yellow subsets in Fig. 5A). When we compared differentiated HDAC1 (wt) and HDAC1 (dn) mES cells (wtDif/dnDif), there was an increased level of m^6A modification in mRNA encoded by the *Sox4* gene (see the exclusively brown frame in Table 2 and brown subset showing one gene in Fig. 5A).

Discussion

We study the functional properties of FTO and ALKBH5 proteins, m^6A RNA erasers, during mouse development, aging, and differentiation processes. In this case, an interesting observation represents the FTO up-regulation in elder male mice. This phenomenon was well-visible in mouse hearts, brains, lungs, and kidneys (Fig. 2A-D). Also, the differentiation, especially into cardiomyocytes, caused the FTO up-regulation. Conversely, we observed ALKBH5 down-regulation in mouse hearts and brains during embryonic development. Also, Sweaad *et al.* [81] showed an essential role for m^6A RNA in prenatal and postnatal development and cardiovascular pathophysiology, which should have a direct link to the function of FTO and ALKBH5 proteins in this process. Mathiyalagan *et al.* [46] showed that FTO is down-regulated in failing mammalian hearts and hypoxic cardiomyocytes. Here, we observed that in human hearts, there is variability in the FTO protein levels when we compared atria and ventricles, which could be caused by a distinct heart disease (Fig. 3Aa-c). Also, there is likely a connection between a genetic disorder in the dysregulation of these proteins and the formation of interatrial septal defects and obesity.

Mathiyalagan *et al.* [46] documented those changes in the FTO level in failing mouse hearts attenuated the ischemia-induced increase in m^6A RNAs and decreased cardiac contractile function. These authors claimed that the demethylation activity of FTO carries out this pathophysiological event. In beating cardiomyocytes, induced experimentally from mES cells *via* EBs, we also showed that cardiomyogenesis is accompanied by changes in METTL-like proteins, "epigenetic writers," responsible for m^6A in RNA. In particular, the distribution of METTL3/METTL14 proteins in the cell nucleus and cytoplasm differed from those parameters analyzed for the METTL16 protein, which is also responsible for N^6-adenosine methylation in distinct types of RNA [16,57]. Also, Yang *et al.* [82] showed that the level of m^6A modification in RNA was the lowest in the heart of one-day-old mice. Conversely, heart tissues from 7-day-old mice were characterized by the highest global m^6A RNA level. Here, we show that it is also essential to discriminate if the analysis is performed in male or female mice because we found that especially the FTO protein is up-regulated in old male mice compared with female individuals (Fig. 2A-D).

Also, we studied FTO and ALKBH5 protein levels during neurogenesis and observed FTO up-regulation during mES cell differentiation into neuroectoderm. Xu *et al.* [83] found that m^6A RNA levels increased due to the *Alkbh5* gene up-regulation observed in rat's cerebral cortex after middle cerebral artery occlusion and primary neurons after oxygen deprivation/ reoxygenation. We found a very low level of the ALKBH5 protein in mouse brains compared with mES cells, while the FTO protein level was relatively high in this tissue. These data showed a distinction in the levels when we compared FTO and ALKBH5 proteins. According to this observation, it seems likely that FTO has a dominant role in regulating N^6-adenosine methylation in RNA when we studied it in mouse brains, especially experimental animals' hearts.

Also, we focused on the *Nanog* gene functional properties that are known to be linked to pluripotency. In

this case, we observed a decrease in m^6A mRNA encoded by the *Nanog* gene, which we analyzed by RIP-Seq during neuroectodermal differentiation of both HDAC1 (wt) and HDAC1 (dn) mES cells (Table 2). In parallel, there was an increased level of FTO studied during this cell differentiation into neuronal pathway (Fig. 4C). To this fact, it is well-known that in the differentiation process, the *Nanog* gene is down-regulated [35].

Our data showed that the m^6A RNA "erasers," especially FTO, change during cell differentiation. Also, aging is accompanied by changes in the FTO protein level, but the ALKBH5 level remains relatively stable in the organs of aging animals. Here, we show that FTO is an essential protein that regulates aging, cardiomyogenesis, and neuroectodermal differentiation. To this fact, we document that differentiation into neuroectoderm is accompanied by a reduced level of N^6-adenosine methylation in mRNA encoded by genes regulating histone code and RNA processing.

Conflict of Interest

There is no conflict of interest.

Acknowledgements

This work was supported by the Institute of Biophysics of the Czech Academy of Sciences (ICO: 68081707).
We want to thank Dr. Roman Hobza and prof. Boris Vyskot from the Institute of Biophysics, Academy of Sciences of the Czech Republic, v.v.i., for access to the cryo-microtome that was used in this study. We thank Christian Seiser from the Max Perutz Laboratories in Vienna for HDAC1 (wt) and HDAC1 (dn) mES cells. This work was supported by the internal support of the Institute of Biophysics of the Czech Academy of Sciences (68081707).

References

1. Desrosiers R, Friderici K, Rottman F. Identification of methylated nucleosides in messenger RNA from Novikoff hepatoma cells. P Natl Acad Sci USA. 1974; 71:3971-3975. https://doi.org/10.1073/pnas.71.10.3971
2. Lavi S, Shatkin AJ. Methylated simian virus 40-specific RNA from nuclei and cytoplasm of infected BSC-1 cells. P Natl Acad Sci USA. 1975; 72:2012-2016. https://doi.org/10.1073/pnas.72.6.2012
3. Rottman F, Shatkin AJ, Perry RP. Sequences containing methylated nucleotides at the 5' termini of messenger RNAs: possible implications for processing. Cell. 1974; 3:197-199. https://doi.org/10.1016/0092-8674(74)90131-7
4. Wei C, Gershowitz A, Moss B. N6, O2'-dimethyladenosine a novel methylated ribonucleoside next to the 5' terminal of animal cell and virus mRNAs. Nature. 1975; 257:251-253. https://doi.org/10.1038/257251a0
5. Wei CM, Moss B. Nucleotide sequences at the N6-methyladenosine sites of HeLa cell messenger ribonucleic acid. Biochemistry-US. 1977; 16:1672-1676. https://doi.org/10.1021/bi00627a023
6. Fu Y, Dominissini D, Rechavi G, He C. Gene expression regulation mediated through reversible m^6A RNA methylation. Nat Rev Genet. 2014; 15:293-306. https://doi.org/10.1038/nrg3724
7. Patil DP, Chen C-K, Pickering BF, Chow A, Jackson C, Guttman M, Jaffrey SR. m(6)A RNA methylation promotes XIST-mediated transcriptional repression. Nature. 2016; 537:369-373. https://doi.org/10.1038/nature19342
8. Yue Y, Liu J, He C. RNA N6-methyladenosine methylation in post-transcriptional gene expression regulation. Gene Dev. 2015; 29:1343-1355. https://doi.org/10.1101/gad.262766.115
9. Sun W-J, Li J-H, Liu S, Wu J, Zhou H, Qu L-H, Yang J-H. RMBase: a resource for decoding the landscape of RNA modifications from high-throughput sequencing data. Nucleic Acids Res. 2016; 44:D259-265. https://doi.org/10.1093/nar/gkv1036
10. Bokar JA, Shambaugh ME, Polayes D, Matera AG, Rottman FM. Purification and cDNA cloning of the AdoMet-binding subunit of the human mRNA (N6-adenosine)-methyltransferase. RNA (New York, NY). 1997; 3:1233-1247.
11. Liu J, Yue Y, Han D, Wang X, Fu Y, Zhang L, Jia G, Yu M, Lu Z, Deng X, Dai Q, Chen W, He C. A METTL3-METTL14 complex mediates mammalian nuclear RNA N6-adenosine methylation. Nat Chem Biol. 2014; 10:93-95. https://doi.org/10.1038/nchembio.1432
12. Knuckles P, Lence T, Haussmann IU, Jacob D, Kreim N, Carl SH, Masiello I, Hares T, Villaseñor R, Hess D, Andrade-Navarro MA, Biggiogera M, Helm M, *et al.* Zc3h13/Flacc is required for adenosine methylation by bridging the mRNA-binding factor Rbm15/Spenito to the m6A machinery component Wtap/Fl(2)d. Gene Dev. 2018; 32:415-429. https://doi.org/10.1101/gad.309146.117

13. Ping X-L, Sun B-F, Wang L, Xiao W, Yang X, Wang W-J, Adhikari S, Shi Y, Lv Y, Chen Y-S, Zhao X, Li A, Yang Y, *et al.* Mammalian WTAP is a regulatory subunit of the RNA N6-methyladenosine methyltransferase. Cell Res. 2014; 24:177-189. https://doi.org/10.1038/cr.2014.3
14. Schwartz S, Mumbach MR, Jovanovic M, Wang T, Maciag K, Bushkin GG, Mertins P, Ter-Ovanesyan D, Habib N, Cacchiarelli D, Sanjana NE, Freinkman E, Pacold ME, *et al.* Perturbation of m6A writers reveals two distinct classes of mRNA methylation at internal and 5' sites. Cell Rep. 2014; 8:284-296. https://doi.org/10.1016/j.celrep.2014.05.048
15. Pendleton KE, Chen B, Liu K, Hunter OV, Xie Y, Tu BP, Conrad NK. The U6 snRNA m6A Methyltransferase METTL16 Regulates SAM Synthetase Intron Retention. Cell. 2017; 169:824-835.e814. https://doi.org/10.1016/j.cell.2017.05.003
16. Warda AS, Kretschmer J, Hackert P, Lenz C, Urlaub H, Höbartner C, Sloan KE, Bohnsack MT. Human METTL16 is a N6-methyladenosine (m6A) methyltransferase that targets pre-mRNAs and various non-coding RNAs. EMBO Rep. 2017; 18:2004-2014. https://doi.org/10.15252/embr.201744940
17. Luo S, Tong L. Molecular basis for the recognition of methylated adenines in RNA by the eukaryotic YTH domain. P Natl Acad Sci USA. 2014; 111:13834-13839. https://doi.org/10.1073/pnas.1412742111
18. Wang X, Lu Z, Gomez A, Hon GC, Yue Y, Han D, Fu Y, Parisien M, Dai Q, Jia G, Ren B, Pan T, He C. N6-methyladenosine-dependent regulation of messenger RNA stability. Nature. 2014; 505:117-120. https://doi.org/10.1038/nature12730
19. Wang X, Zhao BS, Roundtree IA, Lu Z, Han D, Ma H, Weng X, Chen K, Shi H, He C. N(6)-methyladenosine Modulates Messenger RNA Translation Efficiency. Cell. 2015; 161:1388-1399. https://doi.org/10.1016/j.cell.2015.05.014
20. Xiao W, Adhikari S, Dahal U, Chen Y-S, Hao Y-J, Sun B-F, Sun H-Y, Li A, Ping X-L, Lai W-Y, Wang X, Ma H-L, Huang C-M, *et al.* Nuclear m(6)A Reader YTHDC1 Regulates mRNA Splicing. Mol Cell. 2016; 61:507-519. https://doi.org/10.1016/j.molcel.2016.01.012, https://doi.org/10.1016/j.molcel.2016.03.004
21. Zhang Z, Theler D, Kaminska KH, Hiller M, de la Grange P, Pudimat R, Rafalska I, Heinrich B, Bujnicki JM, Allain FH-T, Stamm S. The YTH domain is a novel RNA binding domain. J Biol Chem. 2010; 285:14701-14710. https://doi.org/10.1074/jbc.M110.104711
22. Alarcón CR, Goodarzi H, Lee H, Liu X, Tavazoie S, Tavazoie SF. HNRNPA2B1 Is a Mediator of m(6)A-Dependent Nuclear RNA Processing Events. Cell. 2015; 162:1299-1308. https://doi.org/10.1016/j.cell.2015.08.011
23. Jia G, Fu Y, Zhao X, Dai Q, Zheng G, Yang Y, Yi C, Lindahl T, Pan T, Yang Y-G, He C. N6-methyladenosine in nuclear RNA is a major substrate of the obesity-associated FTO. Nat Chem Biol. 2011; 7:885-887. https://doi.org/10.1038/nchembio.687
24. Fu Y, Jia G, Pang X, Wang RN, Wang X, Li CJ, Smemo S, Dai Q, Bailey KA, Nobrega MA, Han K-L, Cui Q, He C. FTO-mediated formation of N6-hydroxymethyladenosine and N6-formyladenosine in mammalian RNA. Nat Commun. 2013; 4:1798. https://doi.org/10.1038/ncomms2822
25. Zheng G, Dahl JA, Niu Y, Fedorcsak P, Huang C-M, Li CJ, Vågbø CB, Shi Y, Wang W-L, Song S-H, Lu Z, Bosmans RPG, Dai Q, *et al.* ALKBH5 is a mammalian RNA demethylase that impacts RNA metabolism and mouse fertility. Mol Cell. 2013; 49:18-29. https://doi.org/10.1016/j.molcel.2012.10.015
26. Zhao X, Yang Y, Sun B-F, Shi Y, Yang X, Xiao W, Hao Y-J, Ping X-L, Chen Y-S, Wang W-J, Jin K-X, Wang X, Huang C-M, *et al.* FTO-dependent demethylation of N6-methyladenosine regulates mRNA splicing and is required for adipogenesis. Cell Res. 2014; 24:1403-1419. https://doi.org/10.1038/cr.2014.151
27. Cao Y, Zhuang Y, Chen J, Xu W, Shou Y, Huang X, Shu Q, Li X. Dynamic effects of Fto in regulating the proliferation and differentiation of adult neural stem cells of mice. Hum Mol Genet. 2020; 29:727-735. https://doi.org/10.1093/hmg/ddz274
28. Wang X, Huang N, Yang M, Wei D, Tai H, Han X, Gong H, Zhou J, Qin J, Wei X, Chen H, Fang T, Xiao H. FTO is required for myogenesis by positively regulating mTOR-PGC-1α pathway-mediated mitochondria biogenesis. Cell Death Dis. 2017; 8:e2702. https://doi.org/10.1038/cddis.2017.122

29. Li Z, Weng H, Su R, Weng X, Zuo Z, Li C, Huang H, Nachtergaele S, Dong L, Hu C, Qin X, Tang L, Wang Y, *et al*. FTO Plays an Oncogenic Role in Acute Myeloid Leukemia as a N6-Methyladenosine RNA Demethylase. Cancer Cell. 2017; 31:127-141. https://doi.org/10.1016/j.ccell.2016.11.017
30. Su R, Dong L, Li Y, Gao M, Han L, Wunderlich M, Deng X, Li H, Huang Y, Gao L, Li C, Zhao Z, Robinson S, *et al*. Targeting FTO suppresses cancer stem cell maintenance and immune evasion. Cancer Cell. 2020; 38:79-96.e11. https://doi.org/10.1016/j.ccell.2020.04.017
31. Cui Q, Shi H, Ye P, Li L, Qu Q, Sun G, Sun G, Lu Z, Huang Y, Yang C-G, Riggs AD, He C, Shi Y. m6A RNA methylation regulates the self-renewal and tumorigenesis of glioblastoma stem cells. Cell Rep. 2017; 18:2622-2634. https://doi.org/10.1016/j.celrep.2017.02.059
32. Huff S, Tiwari SK, Gonzalez GM, Wang Y, Rana TM. m6A-RNA Demethylase FTO inhibitors impair self-renewal in glioblastoma stem cells. ACS Chem Biol. 2021; 16:324-333. https://doi.org/10.1021/acschembio.0c00841
33. Mauer J, Luo X, Blanjoie A, Jiao X, Grozhik AV, Patil DP, Linder B, Pickering BF, Vasseur J-J, Chen Q, Gross SS, Elemento O, Debart F, *et al.* Reversible methylation of m6Am in the 5' cap controls mRNA stability. Nature. 2017; 541:371-375. https://doi.org/10.1038/nature21022
34. Mauer J, Sindelar M, Despic V, Guez T, Hawley BR, Vasseur J-J, Rentmeister A, Gross SS, Pellizzoni L, Debart F, Goodarzi H, Jaffrey SR. FTO controls reversible m6Am RNA methylation during snRNA biogenesis. Nat Chem Biol. 2019; 15:340-347. https://doi.org/10.1038/s41589-019-0231-8
35. Meyer KD. m(6)A-mediated translation regulation. BBA-Gene Regul Mech. 2019; 1862:301-309. https://doi.org/10.1016/j.bbagrm.2018.10.006
36. Ke S, Pandya-Jones A, Saito Y, Fak JJ, Vågbø CB, Geula S, Hanna JH, Black DL, Darnell JE, Darnell RB. m6A mRNA modifications are deposited in nascent pre-mRNA and are not required for splicing but do specify cytoplasmic turnover. Gene Dev. 2017; 31:990-1006. https://doi.org/10.1101/gad.301036.117
37. Sommer S, Lavi U, Darnell JE. The absolute frequency of labeled N-6-methyladenosine in HeLa cell messenger RNA decreases with label time. J Mol Biol. 1978; 124:487-499. https://doi.org/10.1016/0022-2836(78)90183-3
38. Zou S, Toh JDW, Wong KHQ, Gao Y-G, Hong W, Woon ECY. N(6)-Methyladenosine: a conformational marker that regulates the substrate specificity of human demethylases FTO and ALKBH5. Sci Rep-UK. 2016; 6:25677. https://doi.org/10.1038/srep25677
39. Meyer KD, Saletore Y, Zumbo P, Elemento O, Mason CE, Jaffrey SR. Comprehensive analysis of mRNA methylation reveals enrichment in 3' UTRs and near stop codons. Cell. 2012; 149:1635-1646. https://doi.org/10.1016/j.cell.2012.05.003
40. Bartosovic M, Molares HC, Gregorova P, Hrossova D, Kudla G, Vanacova S. N6-methyladenosine demethylase FTO targets pre-mRNAs and regulates alternative splicing and 3'-end processing. Nucleic Acids Res. 2017; 45:11356-11370. https://doi.org/10.1093/nar/gkx778
41. Aas A, Isakson P, Bindesbøll C, Alemu EA, Klungland A, Simonsen A. Nucleocytoplasmic Shuttling of FTO Does Not Affect Starvation-Induced Autophagy. PLoS One. 2017; 12:e0168182. https://doi.org/10.1371/journal.pone.0168182
42. Gulati P, Avezov E, Ma M, Antrobus R, Lehner P, O'Rahilly S, Yeo GSH. Fat mass and obesity-related (FTO) shuttles between the nucleus and cytoplasm. Bioscience Rep. 2014; 34:e00144. https://doi.org/10.1042/BSR20140111
43. Wei J, Liu F, Lu Z, Fei Q, Ai Y, He PC, Shi H, Cui X, Su R, Klungland A, Jia G, Chen J, He C. Differential m6A, m6Am, and m1A Demethylation Mediated by FTO in the Cell Nucleus and Cytoplasm. Mol Cell. 2018; 71:973-985.e975. https://doi.org/10.1016/j.molcel.2018.08.011
44. Dorn LE, Lasman L, Chen J, Xu X, Hund TJ, Medvedovic M, Hanna JH, van Berlo JH, Accornero F. The N6-Methyladenosine mRNA Methylase METTL3 Controls Cardiac Homeostasis and Hypertrophy. Circulation. 2019; 139:533-545. https://doi.org/10.1161/CIRCULATIONAHA.118.036146
45. Kmietczyk V, Riechert E, Kalinski L, Boileau E, Malovrh E, Malone B, Gorska A, Hofmann C, Varma E, Jürgensen L, Kamuf-Schenk V, Altmüller J, Tappu R, *et al.* m6A-mRNA methylation regulates cardiac gene expression and cellular growth. Life Sci Alliance. 2019; 2:e201800233. https://doi.org/10.26508/lsa.201800233

46. Mathiyalagan P, Adamiak M, Mayourian J, Sassi Y, Liang Y, Agarwal N, Jha D, Zhang S, Kohlbrenner E, Chepurko E, Chen J, Trivieri MG, Singh R, *et al.* FTO-Dependent N6-Methyladenosine Regulates Cardiac Function During Remodeling and Repair. Circulation. 2019; 139:518-532. https://doi.org/10.1161/CIRCULATIONAHA.118.033794
47. Gan XT, Zhao G, Huang CX, Rowe AC, Purdham DM, Karmazyn M. Identification of fat mass and obesity associated (FTO) protein expression in cardiomyocytes: regulation by leptin and its contribution to leptin-induced hypertrophy. PLoS One. 2013; 8:e74235. https://doi.org/10.1371/journal.pone.0074235
48. Berulava T, Buchholz E, Elerdashvili V, Pena T, Islam MR, Lbik D, Mohamed BA, Renner A, von Lewinski D, Sacherer M, Bohnsack KE, Bohnsack MT, Jain G, *et al.* Changes in m6A RNA methylation contribute to heart failure progression by modulating translation. Eur J Heart Fail. 2020; 22:54-66. https://doi.org/10.1002/ejhf.1672
49. Cecil JE, Tavendale R, Watt P, Hetherington MM, Palmer CNA. An obesity-associated FTO gene variant and increased energy intake in children. New Engl J Med. 2008; 359:2558-2566. https://doi.org/10.1056/NEJMoa0803839
50. Haupt A, Thamer C, Staiger H, Tschritter O, Kirchhoff K, Machicao F, Häring H-U, Stefan N, Fritsche A. Variation in the FTO gene influences food intake but not energy expenditure. Exp Clin Endocr Diab. 2009; 117:194-197. https://doi.org/10.1055/s-0028-1087176
51. Smemo S, Tena JJ, Kim K-H, Gamazon ER, Sakabe NJ, Gómez-Marín C, Aneas I, Credidio FL, Sobreira DR, Wasserman NF, Lee JH, Puviindran V, Tam D, *et al.* Obesity-associated variants within FTO form long-range functional connections with IRX3. Nature. 2014; 507:371-375. https://doi.org/10.1038/nature13138
52. Stratigopoulos G, Martin Carli JF, O'Day DR, Wang L, Leduc CA, Lanzano P, Chung WK, Rosenbaum M, Egli D, Doherty DA, Leibel RL. Hypomorphism for RPGRIP1L, a ciliary gene vicinal to the FTO locus, causes increased adiposity in mice. Cell Metab. 2014; 19:767-779. https://doi.org/10.1016/j.cmet.2014.04.009
53. Church C, Moir L, McMurray F, Girard C, Banks GT, Teboul L, Wells S, Brüning JC, Nolan PM, Ashcroft FM, Cox RD. Overexpression of Fto leads to increased food intake and results in obesity. Nat Genet. 2010; 42:1086-1092. https://doi.org/10.1038/ng.713
54. Lavie CJ, De Schutter A, Parto P, Jahangir E, Kokkinos P, Ortega FB, Arena R, Milani RV. Obesity and Prevalence of Cardiovascular Diseases and Prognosis-The Obesity Paradox Updated. Prog Cardiovasc Dis. 2016; 58:537-547. https://doi.org/10.1016/j.pcad.2016.01.008
55. Lavie CJ, Sharma A, Alpert MA, De Schutter A, Lopez-Jimenez F, Milani RV, Ventura HO. Update on Obesity and Obesity Paradox in Heart Failure. Prog Cardiovasc Dis. 2016; 58:393-400. https://doi.org/10.1016/j.pcad.2016.01.008, https://doi.org/10.1016/j.pcad.2015.12.003
56. Liu C, Mou S, Pan C. The FTO gene rs9939609 polymorphism predicts risk of cardiovascular disease: a systematic review and meta-analysis. PLoS One. 2013; 8:e71901. https://doi.org/10.1371/journal.pone.0071901
57. Arcidiacono OA, Krejci J, Bartova E. The distinct function and localization of METTL3/METTL14 and METTL16 enzymes in cardiomyocytes. Int J Mol Sci. 2020; 21. https://doi.org/10.3390/ijms21218139
58. Frayling TM, Timpson NJ, Weedon MN, Zeggini E, Freathy RM, Lindgren CM, Perry JR, Elliott KS, Lango H, Rayner NW, Shields B, Harries LW, Barrett JC, *et al.* A common variant in the FTO gene is associated with body mass index and predisposes to childhood and adult obesity. Science. 2007; 316:889-894. https://doi.org/10.1126/science.1141634
59. Ran S, Jiang Z-X, He X, Liu Y, Zhang Y-X, Zhang L, Pei Y-F, Zhang M, Hai R, Gu G-S, Liu B-L, Tian Q, Zhang Y-H, *et al.* Replication of FTO Gene associated with lean mass in a Meta-Analysis of Genome-Wide Association Studies. Sci Rep-UK. 2020; 10:5057. https://doi.org/10.1038/s41598-020-61406-3
60. Lu D-f, Wang Y, Su Z-z, Zeng Z-h, Xing X-w, He Z-y, Zhang C. Knockdown of the HDAC1 promotes the directed differentiation of bone mesenchymal stem cells into cardiomyocytes. PLoS One. 2014; 9:e92179. https://doi.org/10.1371/journal.pone.0092179
61. Lu D-f, Yao Y, Su Z-z, Zeng Z-h, Xing X-w, He Z-y, Zhang C. Downregulation of HDAC1 Is Involved in the Cardiomyocyte Differentiation from Mesenchymal Stem Cells in a Myocardial Microenvironment. PLoS One. 2014; 9:e93222. https://doi.org/10.1371/journal.pone.0093222

62. Doetschman TC, Eistetter H, Katz M, Schmidt W, Kemler R. The in vitro development of blastocyst-derived embryonic stem cell lines: formation of visceral yolk sac, blood islands and myocardium. J Embryol Exp Morph. 1985; 87:27-45. https://doi.org/10.1242/dev.87.1.27
63. Večeřa J, Bártová E, Krejčí J, Legartová S, Komůrková D, Rudá-Kučerová J, Štark T, Dražanová E, Kašpárek T, Šulcová A, Dekker FJ, Szymanski W, Seiser C, *et al.* HDAC1 and HDAC3 underlie dynamic H3K9 acetylation during embryonic neurogenesis and in schizophrenia-like animals. J Cell Physiol. 2018; 233:530-548. https://doi.org/10.1002/jcp.25914
64. Zupkovitz G, Grausenburger R, Brunmeir R, Senese S, Tischler J, Jurkin J, Rembold M, Meunier D, Egger G, Lagger S, Chiocca S, Propst F, Weitzer G, *et al.* The cyclin-dependent kinase inhibitor p21 is a crucial target for histone deacetylase 1 as a regulator of cellular proliferation. Mol Cell Biol. 2010; 30:1171-1181. https://doi.org/10.1128/MCB.01500-09
65. Keller GM. In vitro differentiation of embryonic stem cells. Curr Opin Cell Biol. 1995; 7:862-869. https://doi.org/10.1016/0955-0674(95)80071-9
66. Robertson EJ. Derivation and maintenance of embryonic stem cell cultures. Methods Mol Biol. 1990; 5:223-236. https://doi.org/10.1385/0-89603-150-0:223
67. Pacherník J, Bryja V, Esner M, Hampl A, Dvorák P. Retinoic acid-induced neural differentiation of P19 embryonal carcinoma cells is potentiated by leukemia inhibitory factor. Physiol Res. 2005; 54:257-262. https://doi.org/10.33549/physiolres.930705
68. Pacherník J, Esner M, Bryja V, Dvorák P, Hampl A. Neural differentiation of mouse embryonic stem cells grown in monolayer. Reprod Nutr Dev. 2002; 42:317-326. https://doi.org/10.1051/rnd:2002028
69. Lian X, Hsiao C, Wilson G, Zhu K, Hazeltine LB, Azarin SM, Raval KK, Zhang J, Kamp TJ, Palecek SP. Robust cardiomyocyte differentiation from human pluripotent stem cells *via* temporal modulation of canonical Wnt signaling. P Natl Acad Sci USA. 2012; 109:E1848-1857. https://doi.org/10.1073/pnas.1200250109
70. Krejcí J, Harnicarová A, Kůrová J, Uhlírová R, Kozubek S, Legartová S, Hájek R, Bártová E. Nuclear organization of PML bodies in leukaemic and multiple myeloma cells. Leukemia Res. 2008; 32:1866-1877. https://doi.org/10.1016/j.leukres.2008.04.021
71. Bolger AM, Lohse M, Usadel B. Trimmomatic: a flexible trimmer for Illumina sequence data. Bioinformatics. 2014; 30:2114-2120. https://doi.org/10.1093/bioinformatics/btu170
72. Dobin A, Davis CA, Schlesinger F, Drenkow J, Zaleski C, Jha S, Batut P, Chaisson M, Gingeras TR. STAR: ultrafast universal RNA-seq aligner. Bioinformatics. 2013; 29:15-21. https://doi.org/10.1093/bioinformatics/bts635
73. Liao Y, Smyth GK, Shi W. featureCounts: an efficient general purpose program for assigning sequence reads to genomic features. Bioinformatics. 2014; 30:923-930. https://doi.org/10.1093/bioinformatics/btt656
74. Cui X, Zhang L, Meng J, Rao MK, Chen Y, Huang Y. MeTDiff: A Novel Differential RNA Methylation Analysis for MeRIP-Seq Data. IEEE/ACM Trans Comput Biol Bioinform. 2018; 15:526-534. https://doi.org/10.1109/TCBB.2015.2403355
75. Conway JR, Lex A, Gehlenborg N. UpSetR: an R package for the visualization of intersecting sets and their properties. Bioinformatics. 2017; 33:2938-2940. https://doi.org/10.1093/bioinformatics/btx364
76. Maltsev VA, Rohwedel J, Hescheler J, Wobus AM. Embryonic stem cells differentiate in vitro into cardiomyocytes representing sinusnodal, atrial and ventricular cell types. Mech Develop. 1993; 44:41-50. https://doi.org/10.1016/0925-4773(93)90015-P
77. Robbins J, Gulick J, Sanchez A, Howles P, Doetschman T. Mouse embryonic stem cells express the cardiac myosin heavy chain genes during development in vitro. J Biol Chem. 1990; 265:11905-11909. https://doi.org/10.1016/S0021-9258(19)38485-6
78. Zhao Y, Chen Y, Jin M, Wang J. The crosstalk between m6A RNA methylation and other epigenetic regulators: a novel perspective in epigenetic remodeling. Theranostics. 2021; 11:4549-4566. https://doi.org/10.7150/thno.54967
79. Ward JM, Elmore SA, Foley JF. Pathology Methods for the Evaluation of Embryonic and Perinatal Developmental Defects and Lethality in Genetically Engineered Mice. Vet Pathol. 2012; 49:71-84. https://doi.org/10.1177/0300985811429811

80. Ke S, Alemu EA, Mertens C, Gantman EC, Fak JJ, Mele A, Haripal B, Zucker-Scharff I, Moore MJ, Park CY, Vågbø CB, Kusśnierczyk A, Klungland A, *et al.* A majority of m 6 A residues are in the last exons, allowing the potential for 3′ UTR regulation. Gene Dev. 2015; 29:2037-2053. https://doi.org/10.1101/gad.269415.115
81. Sweaad WK, Stefanizzi FM, Chamorro-Jorganes A, Devaux Y, Emanueli C. Relevance of N6-methyladenosine regulators for transcriptome: Implications for development and the cardiovascular system. J Mol Cell Cardiol. 2021; 160:56-70. https://doi.org/10.1016/j.yjmcc.2021.05.006
82. Yang Y, Shen S, Cai Y, Zeng K, Liu K, Li S, Zeng L, Chen L, Tang J, Hu Z, Xia Z, Zhang L. Dynamic Patterns of N6-Methyladenosine Profiles of Messenger RNA Correlated with the Cardiomyocyte Regenerability during the Early Heart Development in Mice. Oxid Med Cell Longev. 2021; 2021:5537804. https://doi.org/10.1155/2021/5537804
83. Xu K, Mo Y, Li D, Yu Q, Wang L, Lin F, Kong C, Balelang MF, Zhang A, Chen S, Dai Q, Wang J. N6-methyladenosine demethylases Alkbh5/Fto regulate cerebral ischemia-reperfusion injury. Ther Adv Chronic Dis. 2020; 11:2040622320916024. https://doi.org/10.1177/2040622320916024